Climate variability leads to multiple oxygenation episodes across the great oxidation event

Daniel Garduno Ruiz, Colin Goldblatt, and Anne-Sofie Ahm

2024

Geophysical Research Letters

RESEARCH LETTER
10.1029/2023GL106694

Climate Variability Leads to Multiple Oxygenation Episodes Across the Great Oxidation Event

Daniel Garduno Ruiz[1], **Colin Goldblatt**[1], **and Anne-Sofie Ahm**[1]

[1]School of Earth and Ocean Sciences, University of Victoria, Victoria, BC, Canada

Key Points:

- Across the Great Oxidation Event (GOE), extreme climate change linked to global glaciations can drive oscillations in atmospheric O_2 levels and mass-independent fractionation of sulfur isotopes (MIF-S) production
- Glacial climates and hot-moist greenhouse climates were likely characterized by pre-GOE and post-GOE O_2 levels respectively
- Temperature changes associated with global glaciations can help explain the MIF-S record across the GOE

Supporting Information:

Supporting Information may be found in the online version of this article.

Correspondence to:

D. G. Ruiz,
danielgardunoruiz@uvic.ca

Citation:

Ruiz, D. G., Goldblatt, C., & Ahm, A.-S. (2024). Climate variability leads to multiple oxygenation episodes across the Great Oxidation Event. *Geophysical Research Letters*, *51*, e2023GL106694. https://doi.org/10.1029/2023GL106694

Received 5 OCT 2023
Accepted 14 JAN 2024

Author Contributions:

Conceptualization: Colin Goldblatt
Funding acquisition: Colin Goldblatt, Anne-Sofie Ahm
Investigation: Daniel Garduno Ruiz, Colin Goldblatt
Methodology: Daniel Garduno Ruiz, Colin Goldblatt, Anne-Sofie Ahm
Software: Daniel Garduno Ruiz
Supervision: Colin Goldblatt, Anne-Sofie Ahm
Visualization: Daniel Garduno Ruiz
Writing – original draft: Daniel Garduno Ruiz
Writing – review & editing: Colin Goldblatt, Anne-Sofie Ahm

Abstract The temporal relationship between global glaciations and the Great Oxidation Event (GOE) suggests that climate change played an important role in Earth's oxygenation. The potential role of temperature is captured by the stratigraphic proximity between glacial deposits and sediments containing mass-independent fractionation of sulfur isotopes (MIF-S). We use a time-dependent one-dimensional photochemical model to investigate whether temperature changes associated with global glaciations can drive oscillations in atmospheric O_2 levels and MIF-S production across the GOE. We find that extreme climate change can cause atmospheric O_2 to oscillate between pre ($<10^{-6}$ times the present atmospheric level, PAL) and post-GOE ($>10^{-5}$ PAL) levels. Post-glacial hot-moist greenhouse climates lead to post-GOE O_2 levels because the abundant H_2O vapor and oxidizing radicals drive the depletion of reduced species. This pattern is generally consistent with the MIF-S signal observed in the sedimentary record, suggesting a link between global glaciations and O_2 oscillations across the GOE.

Plain Language Summary The Great Oxidation Event was the most significant environmental and chemical transformation in Earth's history, marking the first time oxygen accumulated in the atmosphere around 2.4 billion years ago. Oxygen increased from below one millionth (low) to at least one-thousandth of a percent (intermediate) of the present oxygen concentration during this event. However, measurements of geochemical oxygen proxies suggest that oxygen levels oscillated between low and intermediate levels before stabilizing after this event. The first rise of atmospheric oxygen occurred during a period of extreme climate variability indicated by the presence of glacial rock deposits around this time. In this study, we use a time-dependent photochemical model to show that extreme temperature changes caused by global glaciations can drive oscillations in atmospheric oxygen levels across the Great Oxidation Event (GOE). Our results can help explain why atmospheric oxygen shows drastic changes across the GOE in a way that is consistent with the geochemical record.

1. Introduction

One of the most fundamental changes to Earth's atmosphere occurred ~2.4 billion years ago during the Great Oxidation Event (GOE) when oxygen first rose to levels $>10^{-6}$ times the present atmospheric level, and the ozone layer finally formed (D. C. Catling & Zahnle, 2020; Zahnle et al., 2006). During the same period, Earth's climate underwent dramatic changes with multiple global scale glaciations, so-called snowball Earth events (Rasmussen et al., 2013). The geological record demonstrates that these changes in climate and oxygen were closely related, as recorded by the stratigraphic proximity between glacial deposits and swings in the record of mass-independent fractionation of sulfur isotopes (MIF-S, Gumsley et al. (2017); Poulton et al. (2021)). In this paper, we will explore whether the effect of extreme climate change on photochemical reactions can cause oxygen fluctuations across the GOE.

The GOE is expressed globally through various geological and geochemical indicators, but the main line of evidence for an O_2 increase during the GOE comes from the MIF-S record. The MIF-S signal forms under anoxic photochemistry in the atmosphere and is transferred to rocks through deposition of S_8 aerosols and sulfate particles (Farquhar et al., 2000, 2001; Pavlov & Kasting, 2002). The geological record shows that MIF-S deposition stopped between 2.5 and 2.3 billion years ago (Ga), suggesting that atmospheric O_2 levels increased above 10^{-6} times the present atmospheric level (PAL) around this time (D. C. Catling & Zahnle, 2020; Zahnle et al., 2006).

The GOE is correlated with extreme climate changes. Up to four glacial deposits surround the transition to an oxygenated atmosphere in South Africa, North America, and Australia (Tang & Chen, 2013). Correlation

between the glacial deposits and low paleo-latitude evidence suggests three of these glaciations may represent global snowball Earth events (Evans et al., 1997; Rasmussen et al., 2013; Williams & Schmidt, 1997). The global glaciations reached surface temperatures below 250K (Abbot et al., 2013) and were likely followed by hot-moist greenhouse climates characterized by temperatures above 320K (Kirschvink, 1992; Popp et al., 2016). Photochemical models suggest that this extreme climate variability affected the evolution of atmospheric O_2 across the GOE through changes in water vapor and the production of oxidizing radicals, leading to variations in O_2 and O_3 levels of up to three orders of magnitude after the GOE (Garduno Ruiz et al., 2023). Consequently, climate variability could be important in explaining MIF-S swings across the GOE.

The appearance and disappearance of the MIF-S signal in the South African Kapvaal craton suggest that atmospheric O_2 oscillated between pre and post-GOE levels across the transition to an oxygenated atmosphere. These MIF-S swings have been explained as a consequence of the dynamic interplay between changes in weathering, the input flux of nutrients to the oceans, and methane oxidation (Gumsley et al., 2017; Poulton et al., 2021).

Here, we use a time-dependent one-dimensional photochemical model (Wogan et al., 2022) to investigate if temperature change associated with the Paleoproterozoic Huronian glaciations can trigger oscillations in atmospheric O_2 levels across the GOE. We find that extreme climate change could explain some of the MIF-S swings present in the rock record. This paper builds on results from a previous study (Garduno Ruiz et al., 2023), which considered photochemical steady-state atmospheres to investigate the effect of temperature on O_2 levels. In this paper, we specifically investigate the transient evolution, and explore how temperature changes over time affect O_2 levels surrounding the GOE.

2. Methods

We use a time-dependent one-dimensional photochemical model (Archean template, Wogan et al. (2022)) to explore if temperature changes caused by global glaciations can cause oscillations in oxygen levels and MIF-S production across the GOE. Our modeling considers the effect of temperature change in atmospheric photochemistry without considering the effect on climate.

We use our simulations to evaluate the production of MIF-S across glacial and hot-moist greenhouse periods. We assume that MIF-S can be transferred to sediments when S_8 aerosols are an important product of atmospheric photochemistry. This condition is satisfied when O_2 mixing ratios are lower than 10^{-7} (Wogan et al., 2022; Zahnle et al., 2006). For higher O_2 levels, the S_8 column goes to zero and we assume that MIF-S production stops.

2.1. Atmospheric Structure

We represent the temperature profile using a moist-adiabatic troposphere merged with a 215K isothermal stratosphere. At different surface temperatures we adjust the surface pressure and the height of the tropopause to account for the change in water vapor content (Garduno Ruiz et al., 2023). We use a constant relative humidity profile of 0.35 in the troposphere. We chose this profile because it is the simplest profile that approximates the observed globally averaged relative humidity profile (Abraham & Goldblatt, 2023), and because using a more complex and realistic relative humidity profile with a strong humidity gradient at the boundary layer results in numerical problems in the photochemical model. In all our simulations we keep a constant CH_4 to O_2 flux ratio of 0.49 because this ratio is considered representative of the Archean (D. Catling et al., 2007).

2.2. Steady States Parameter Space

To explore how the model reacts to temperature and O_2 flux changes, we first define a parameter space of steady state O_2 levels at different prescribed surface O_2 fluxes and temperatures. To construct this parameter space, we run the model to steady state at surface temperatures ranging from 250 to 350K (with an initial value of 290K), and O_2 surface fluxes ranging from 10^{12} to 10^{13} molecules/cm^2/s (henceforth /cm^2/s). The results are described in Section 3.1.

2.3. Time-Dependent Simulations

We subsequently prescribe a surface temperature evolution that simulates the effect of global glaciations on temperature. We characterize temperate climates with a temperature of 290K that drops to 250K during the

glaciations (Abbot et al., 2013), assuming that the glacial events spanned 10 million years (My). We use the glacial deposits age constraints complied in Gumsley et al. (2017) and Bekker et al. (2020). After the glaciations, we increase the surface temperature to 320K to simulate a glacial exit to a hot-moist greenhouse climate (Popp et al., 2016). Finally, we simulate the return to temperate 290K conditions following a sigmoid-like decline in 10 My because some modeling studies suggest that the post-glacial moist-greenhouse state likely spanned a few million years (Hir et al., 2009), if not tens of millions of years (Mills et al., 2011).

We integrate the photochemical model over time as an initial value problem with the CVODE integration method (Wogan et al., 2022). We run the model in 10^5 year intervals, assuming that temperature remains constant across each 10^5 year window. At each 10^5 year interval, we update the temperature and eddy diffusivity profiles, and surface pressure, according to our prescribed surface temperature evolution.

We consider three scenarios in which we prescribe different O_2 and reductant input fluxes over time. Our results are not very sensitive to the specific fluxes we choose in these scenarios. The goal of this manuscript is not to constrain absolute flux values.

2.3.1. Time Dependent Temperature Forcing With a Constant O_2 Flux

To isolate the effect of temperature changes on O_2 levels, we run the model with constant O_2 input fluxes of 1.8×10^{12}/cm^2/s and 2.2×10^{12}/cm^2/s. We choose these fluxes to illustrate different model responses to temperature changes depending on the O_2 flux. We keep the reductant input flux at a constant value of 3.3×10^{10}/cm^2/s (Zahnle et al., 2006).

2.3.2. Time Dependent Temperature Forcing With a Linear Increase in O_2 Flux

We consider two cases. First, we prescribe a linear O_2 flux increase with a rate of 8.88×10^9/cm^2/s per million years. We arbitrarily choose this rate because it matches some of the available MIF-S constraints across the GOE. Second, we superimpose a decrease of 60% in the O_2 input flux during the glacial periods to simulate a decrease in productivity due to harsh conditions for primary producers, and we add a 60% increase in the O_2 input flux during the hot-moist greenhouse periods to simulate an increase in productivity due to increased nutrient flux to the oceans during deglaciations (Harada et al., 2015). We choose a 60% scale factor to match the MIF-S observations during glacial periods.

2.3.3. Time Dependent Temperature Forcing With a Linear Decrease in Reductant Input Flux

We decrease the reductant input flux from an initial value of 2.2×10^{10}/cm^2/s to a final value of 1×10^{10}/cm^2/s throughout 190 My, keeping a constant CO to H_2 ratio of 0.1 (Zahnle et al., 2006). This decrease in reductant input flux is broadly consistent with previous estimates (Kadoya et al., 2020). Similarly to our O_2 flux increase case (Section 2.3.2), we consider two scenarios for the O_2 input flux evolution. First, we keep a constant 2.2×10^{12}/cm^2/s O_2 input flux. Second, we superimpose a 60% decrease in O_2 input flux during glaciations and a 60% increase during hot-moist greenhouse periods.

3. Results

3.1. Steady States Parameter Space

The steady state parameter space shows three different scenarios where a temperature change will have dramatic effects on the O_2 surface mixing ratio (Figure 1). First, for O_2 fluxes below 2×10^{12}/cm^2/s, increasing temperature from 290K to above 310K leads to post-GOE oxygen levels. At lower O_2 flux values, a bigger increase in temperature is needed to cause oxygenation. Second, for O_2 fluxes between 2×10^{12} and 2.8×10^{12}/cm^2/s, a decrease in temperature from 290K to below 260K also results in oxygenation. While some of the steady states between this flux range display intermediate O_2 levels, these states are very sensitive to small (5%) O_2 flux perturbations and are likely to be unstable. These results suggest that it is unlikely that the atmosphere will remain in those states for long periods. Oxygen fluxes higher than 2.8×10^{12}/cm^2/s result in post-GOE oxygen levels for all temperatures.

The temperature sensitivity of O_3, CH_4, and S_8 aerosols follow the steady state concentration of O_2 (Figure 1). High O_2 concentrations lead to more oxidation and lower CH_4 concentrations. In contrast, since O_3 is a

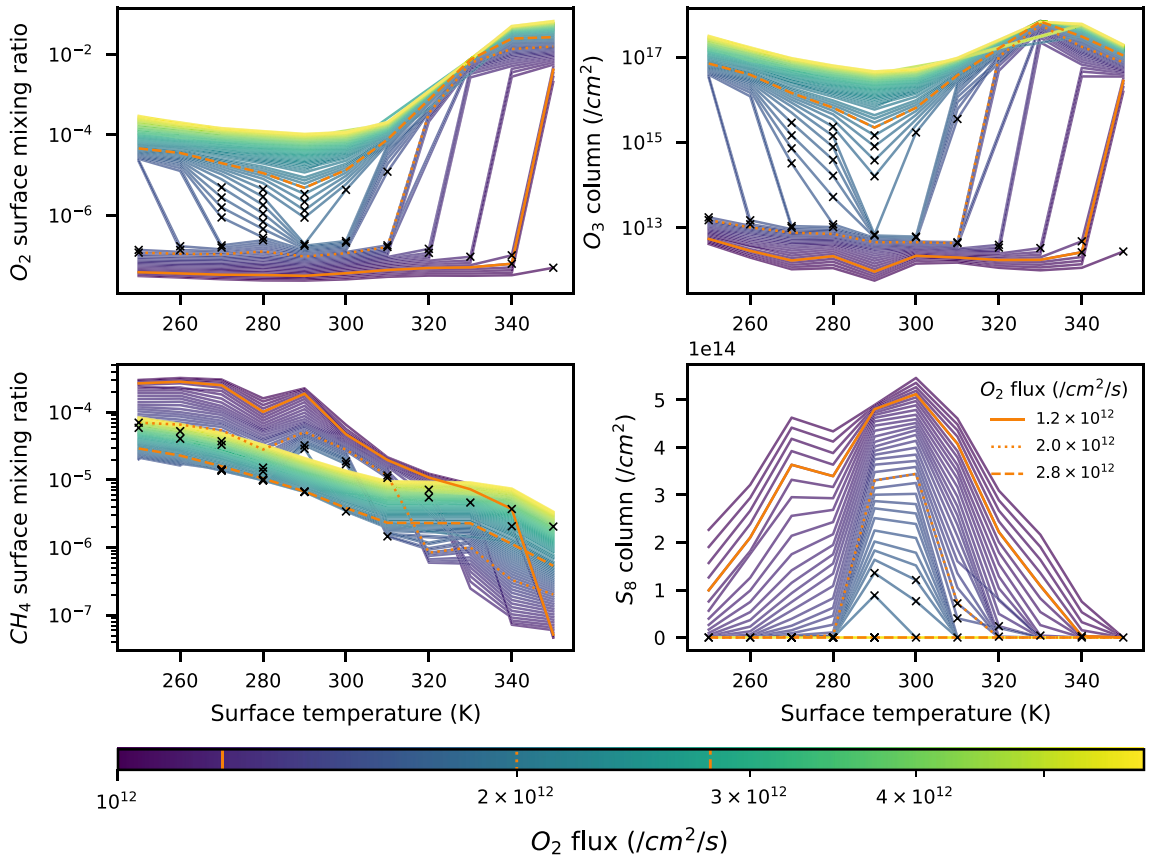

Figure 1. Model defined parameter space of atmospheric steady state O_2 and CH_4 surface mixing ratios, and O_3 and S_8 columns across different prescribed surface O_2 fluxes and temperatures. Three characteristic model scenarios are highlighted with orange lines. The "x" symbols represent steady states that change more than a factor of two with a 5% O_2 flux perturbation. These states are very sensitive to small O_2 flux perturbations and are likely to be unstable.

photochemical product of O_2, the O_3 concentration measured through an integrated column shows the same trends as O_2. The presence of an O_3 layer inhibits the formation of S_8 aerosols, so S_8 aerosols are only present at low O_2 fluxes.

3.2. Time Dependent Temperature Forcing With a Constant O_2 Flux

The time-dependent model simulations demonstrate that temperature changes associated with the Huronian glaciations can drive oscillations in O_2 levels and MIF-S across the GOE. In the first simulation (Figure 2), these oscillations are driven by change in temperature only, as O_2 and reductant input fluxes are kept constant (Section 2.3.1). While these O_2 oscillations are solely driven by the changes in atmospheric chemistry caused by temperature, the specific value of the O_2 input flux controls the time evolution of atmospheric O_2.

The glacial periods are characterized by low or high O_2 levels depending on the O_2 input flux. At an O_2 input flux of 1.8×10^{12}/cm^2/s, the drop in temperature leads to a slight increase in surface O_2 (Figure 2c continuous line). However, at an O_2 input flux of 2.2×10^{12}/cm^2/s, the glaciations cause O_2 to increase from a mixing ratio of 10^{-7} to 10^{-5}, leading to an oxygenated atmosphere, and suppressing the production of MIF-S through S_8 aerosols (Figures 2c and 2e dotted). This behavior results from the decrease in tropospheric and stratospheric water vapor during the glacial periods. Less water vapor results in lower production of oxidizing radicals like OH, leading to lower oxidation rates and less O_2 loss. At an O_2 flux of 1.8×10^{12}/cm^2/s the lower rates of oxidation lead to a small O_2 and O_3 increase in the troposphere (Figures 2f and 2g). While this increase in O_3 concentration also drives a decrease in S_8 aerosol production, it is not enough to eliminate MIF-S across the glacial periods (Figure 2e). In contrast, at an O_2 input flux of 2.2×10^{12}/cm^2/s, the decrease in O_2 loss combined with the higher O_2 input flux cause the establishment of an O_3 layer and oxygenated conditions during glacial periods, terminating MIF-S signals (Figure 2g).

10.1029/2023GL106694

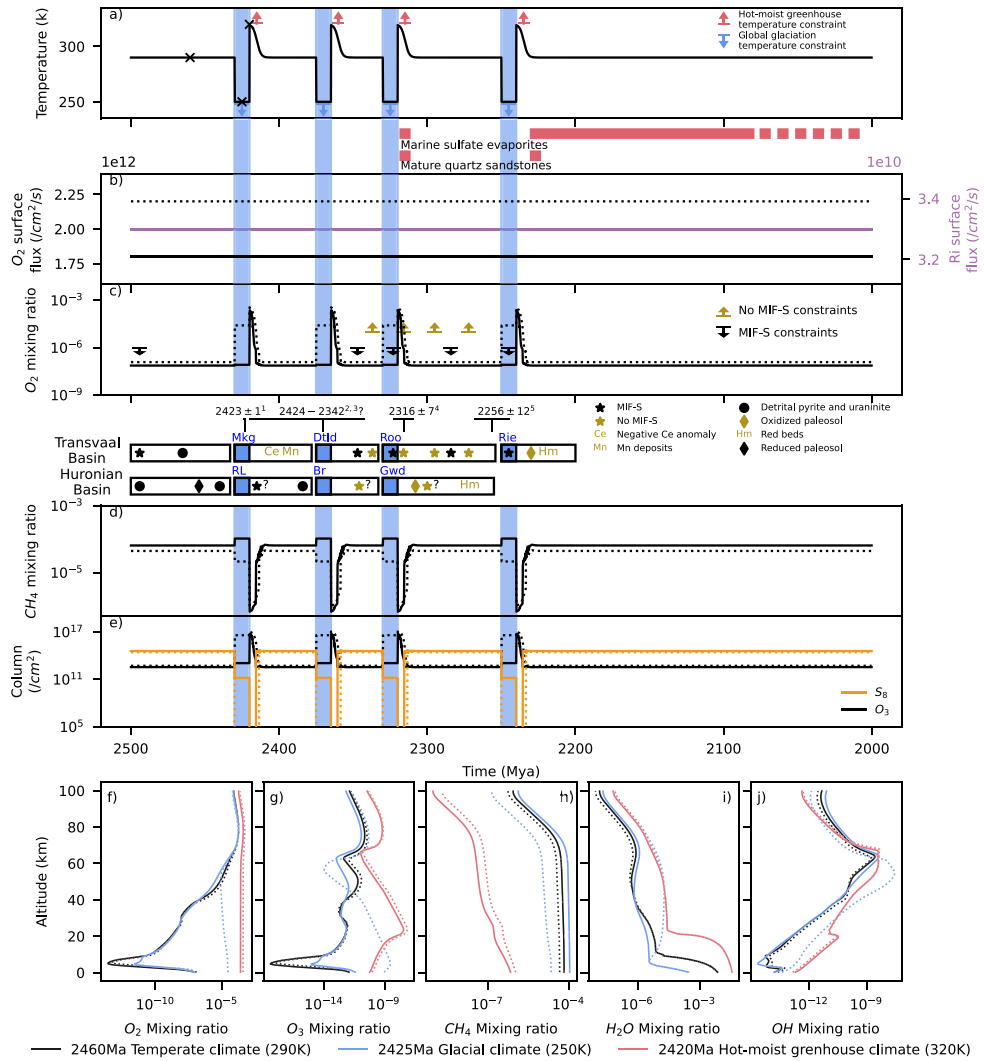

Figure 2. This figure shows two different model scenarios using a similar temperature evolution (a) but with two different constant O_2 input flux values (b). Depending on the initial O_2 input flux value, the O_2 surface mixing ratio (c), CH_4 surface mixing ratio (d), and O_3 and S_8 columns (e) show distinct trends. The four blue vertical bars represent glaciations (Bekker & Holland, 2012; Gumsley et al., 2017; Poulton et al., 2021). The red and blue arrows in panel (a) represent modeling temperature constraints during glacial (Abbot et al., 2013) and hot-moist greenhouse (Popp et al., 2016) periods. The "×" symbols show the points in time where we plot species profiles in panels (f–j). The red horizontal bars show times when evidence of hot climates from marine sulfate evaporites and mature quartz sandstones can be found (Bekker & Holland, 2012; Bekker et al., 2005). In panel (c) the black and gold arrows represent O_2 constraints from MIF-S measurements in the Transvaal basins (Farquhar et al., 2000; Guo et al., 2009; Luo et al., 2016; Poulton et al., 2021). Note that the absolute time of these constraints is not well known. We put these constraints on a time-scale consistent with their position relative to glacial deposits. Redox proxies and their relative position to the glaciations in the Transvaal and Huronian basins are shown below panel (c) (Gumsley et al., 2017). Chronological constraints and their uncertainty near the glacial deposits come from 1. Senger et al. (2023), 2. Schröder et al. (2016), 3. Zeh et al. (2020), 4. Hannah et al. (2004), 5. Rasmussen et al. (2013). The formation name abbreviations are: Mkg (Makganyene), Dtld (Duitschland), Roo (Rooihoogte), Rie (Rietfontein), RL (Ramsay Lake), Br (Bruce), Gwd (Gowganda). In panels (f–j) we show species profiles at points in time shown in "×" symbols in panel (a) during temperate (black), glacial (blue), and hot-moist greenhouse (red) conditions. The profiles line style corresponds to the line style of the O_2 fluxes in panel (b).

The exit of the glaciations to a hot-moist greenhouse climate is characterized by high O_2 mixing ratios of $\sim 5 \times 10^{-4}$ independent of the O_2 input flux values (Figures 2c and 2f). The increase in water vapor during the hot-moist greenhouse conditions boosts the production of oxidizing radicals, leading to the depletion of reduced species like CH_4 and increasing O_2 levels (Figures 2d–2j).

Finally, the return to temperate climates results in the restoration of low O_2 levels. This model result suggests that although temperature changes can drive O_2 oscillations by themselves, an increase in the O_2 input flux or a decrease in reductant input flux over time is necessary to maintain post-GOE O_2 levels at temperate climates.

3.2.1. Atmospheric Chemical Profiles

The temperate, glacial, and hot-moist greenhouse climates have characteristic species profiles that are shaped by the water vapor content of the atmosphere and the O_2 input flux (Figures 2f–2j). First, temperate climates are characterized by low O_2 and O_3 concentrations that reach a minimum near 10 km (Figures 2f and 2g). Second, glacial climates are characterized by decreased water vapor in the troposphere and the stratosphere (Figure 2i). With less water vapor, there is less production of oxidizing radicals and less O_2 consumption. Thus, the O_2 and O_3 profiles show an increase in concentration compared to the temperate climate profiles, resulting in oxygenation and formation of an O_3 layer for the 2.2×10^{12}/cm^2/s O_2 flux case. In this case, after O_2 builds up, the O_3 layer shields H_2O against photochemical destruction, causing an increase in H_2O vapor above the troposphere. The abundant O_2 and H_2O lead to higher OH production via water vapor photolysis and the reaction $H_2O + O(^1D) \rightarrow 2OH$, increasing CH_4 oxidation and decreasing the CH_4 concentration at all altitudes. Third, the hot-moist greenhouse climates are characterized by high water vapor concentrations, leading to abundant oxidizing radicals (Figures 2i and 2j). These radicals react with and deplete CH_4, leading to the oxygenation of the atmosphere and the formation of an O_3 layer.

3.3. Time Dependent Temperature Forcing With a Linear Increase in O_2 Flux

The second time-dependent model simulation (Figure 3) investigates the effect of temperature by using a linear increase in O_2 flux (see Section 2.3.2). Superimposing a 60% decrease during glacial periods results in pre-GOE O_2 levels (Figure 3c continuous). The low O_2 levels during glaciations lead to abundant S_8 production (Figure 3e continuous orange line). In contrast, if these superimposed O_2 flux changes are not included some glacial periods show post-GOE O_2 levels and no S_8 production (Figures 3c and 3e dotted).

3.4. Time Dependent Temperature Forcing With a Linear Decrease in Reductant Input Flux

Driving a gradual increase in O_2 levels with a decrease in reductant input flux (Section 2.3.3) leads to similar results than driving the increase in O_2 levels with an increase in O_2 input flux (Figure 4). In this case, when the O_2 flux is constant, O_2 shows post-GOE levels during glacial and hot moist greenhouse periods (Figure 4c dotted) and the S_8 production stops during the first glaciation (Figure 4e dotted orange line). In contrast, superimposing a 60% decrease in O_2 flux during glacial periods and a 60% increase during hot-moist greenhouse periods leads to pre-GOE O_2 levels during glaciations, and post-GOE O_2 levels after glaciations (Figure 4c continuous). The low O_2 levels facilitate the production of MIF-S through S_8 aerosols during glacial periods, but the decrease in reductant input flux makes the S_8 production decrease over time (Figure 4e continuous orange line). This pattern occurs because S_8 photochemical production requires three conditions: low O_2 levels, enough abundance of reduced gases, and input of sulfur gases to the atmosphere (Zahnle et al., 2006).

4. Discussion

The MIF-S record across the GOE shows a complex pattern. There are positive MIF-S values between the second and third glaciations that disappear before the onset of the third glaciation (Guo et al., 2009). The signal comes back in the glacial deposits and surrounding breccias and conglomerates of the third glaciation and is lost again afterward (Izon et al., 2022; Luo et al., 2016; Poulton et al., 2021). Finally, sparse MIF-S signals occur between the third and fourth glaciations, with some non-zero MIF-S values in the glacial deposits of the fourth glaciation (Poulton et al., 2021).

Our results show that some of the MIF-S swings observed in the rock record can be explained by temperature changes associated with global glaciations. Provided that the O_2 input flux is low (e.g., $<2 \times 10^{12}$/cm^2/s) during glacial periods, our results are consistent with the presence of MIF-S signals in glacial deposits and the disappearance of the signal after the glaciations. Low O_2 fluxes during glacial periods are a reasonable assumption due to the difficult conditions for primary producers. In contrast, the aftermath of the glaciations leads to the loss of the MIF-S signal because the hot-moist greenhouse conditions cause oxygenation. This pattern is observed in the sedimentary record associated with the third (Izon et al., 2022; Luo et al., 2016) and fourth glaciations (Poulton

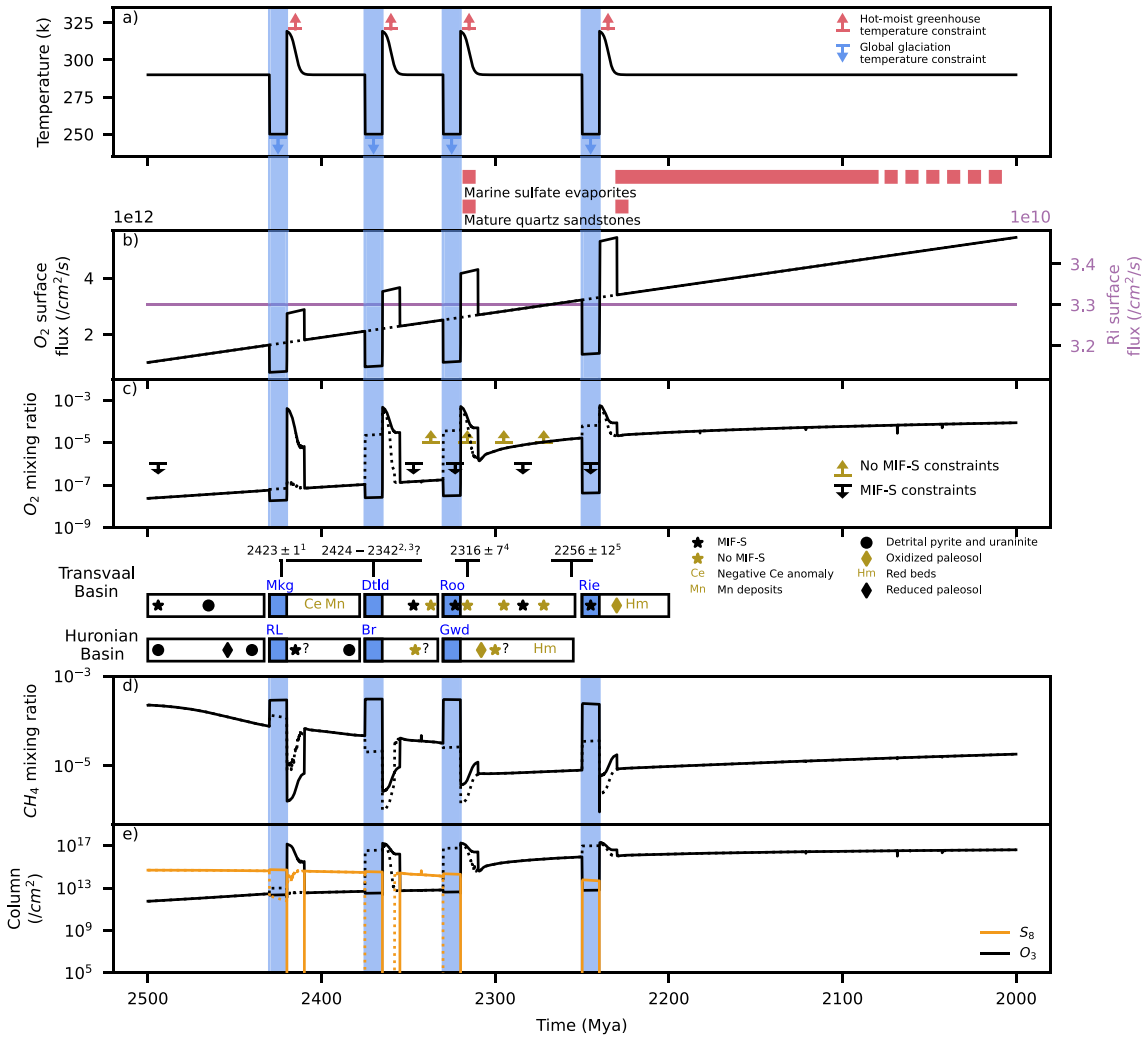

Figure 3. This figure shows two different model scenarios, prescribed with the same temperature evolution (a) but two different O_2 input flux histories (b). First, a linear increase in O_2 input flux over time (dotted line). In this case, as the O_2 input flux increases, the O_2 mixing ratio (c) shows a gradual increase perturbed by temperature changes. The O_2 mixing ratio increases above 10^{-5}, and the S_8 production stops during glaciations and hot-moist greenhouse periods when the flux is $>2.1 \times 10^{12}/cm^2/s$. Second, a linear increase in O_2 input flux that drops 60% during glaciations and increases 60% during hot-moist greenhouse climates. In this case, the decrease in O_2 flux during glaciations leads to low O_2 levels during glacial periods, whereas the increase in temperature and O_2 input flux during hot-moist greenhouse periods lead to high O_2 levels.

et al., 2021). However, there are some MIF-S constraints that we can not explain with temperature changes. For example, the disappearance of the MIF-S signal before the third glaciation and the MIF-S swings between the third and fourth glaciations are difficult to explain with temperature changes alone.

The GOE was a complex event where multiple forcings could have affected the evolution of atmospheric O_2 levels. Changes in biogenic fluxes, massive volcanic eruptions, or changes in the composition of volcanic gases could have altered the concentration of O_2 across the GOE (Kasting, 2013; Wogan et al., 2022). The MIF-S oscillations that are not associated with periods of climate change could represent alterations to the redox budget of the atmosphere from one of these other perturbations.

On the time scales considered in this study (500 My), changes in other redox reservoirs could have affected the evolution of atmospheric O_2. For example, changes in the rate of reduced mineral oxidation in the crust or changes in the rate of volcanic input to the atmosphere could have altered O_2 concentrations. Our modeling implicitly includes external effects on atmospheric redox state by imposing changes in O_2 and reductant input fluxes, but we do not explicitly include interactions between redox reservoirs. Also, our modeling does not explicitly consider the interactions and feedback mechanisms between atmospheric chemistry and climate. For example, our results

10.1029/2023GL106694

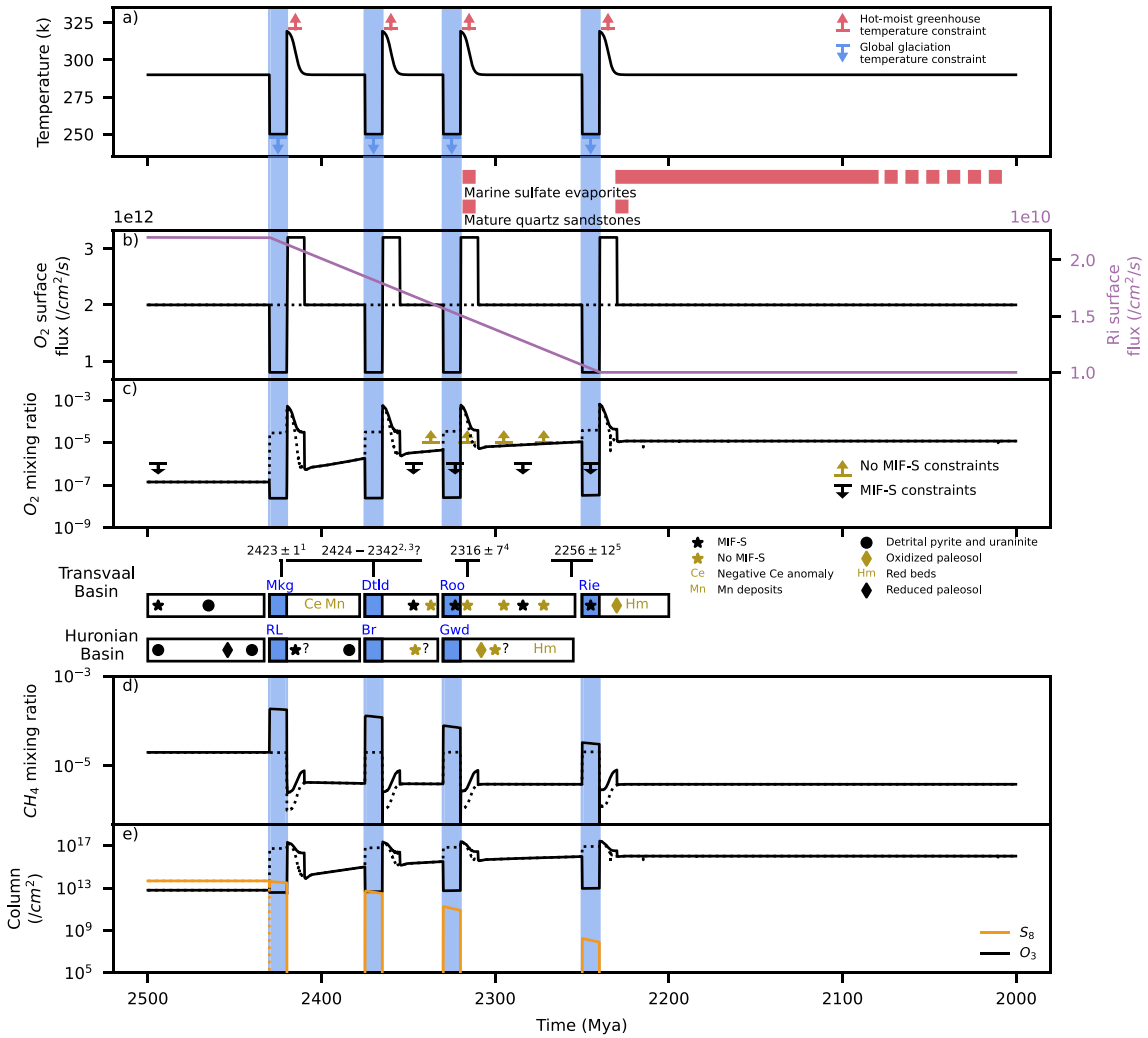

Figure 4. This figure shows a model scenario in which we drive a gradual increase in O_2 levels with a decrease in reductant input flux (purple line in panel b, see Section 2.3.3), considering two O_2 flux histories. First, we keep a constant $2 \times 10^{12}/cm^2/s$ O_2 flux (dotted lines). This case shows O_2 mixing ratios $>10^{-5}$, and no S_8 production during glaciations and hot-moist greenhouse periods. Second, we superimpose a 60% decrease in O_2 flux during glaciations and a 60% increase during hot-moist greenhouse climates (continuous black line in panel b). This case shows low O_2 levels during glacial periods and high O_2 levels during hot-moist greenhouse periods.

show that during hot-moist greenhouse periods, the increase in temperature leads to a decrease of CH_4 mixing ratios from $\sim 10^{-4}$ to $\sim 10^{-6}$ (Figures 2d and 3e). This CH_4 decrease would impact climate, decreasing temperature and going against the effect of the initial temperature increase. Also, the high CO_2 concentration during hot-moist greenhouse periods could enhance the photochemical production of CO, increasing the concentration of reduced species and counteracting the O_2 increase caused by high temperatures. We leave investigation of these feedback mechanisms to a future study.

Our results contrast with recent studies that suggest that the MIF-S swings in the rock record are a product of the recycling of previously produced MIF-S signals (Killingsworth et al., 2019; Philippot et al., 2018; Reinhard et al., 2013). See the Supporting Information S1 for discussion on this topic.

5. Conclusions

We used a time-dependent photochemical model to show that temperature changes associated with the Paleoproterozoic glaciations are a plausible cause of oxygen concentration and MIF-S oscillations across the GOE. The model results demonstrate that the glacial periods associated with the GOE are likely characterized by low O_2

levels due to low O_2 input fluxes. The exit of the glaciations to hot-moist greenhouse climates is characterized by post-GOE O_2 levels, and this increase in atmospheric O_2 can be driven by increasing temperatures alone. These results are consistent with the sedimentary record of MIF-S signals associated with the Paleoproterozoic glacial deposits and support a primary origin for MIF-S generation.

Data Availability Statement

The complete model output can be downloaded at Garduno Ruiz et al. (2024a). All instructions, scripts, and model output necessary to reproduce our results are available at Garduno Ruiz et al. (2024b).

Acknowledgments
We acknowledge and respect the lək̓ʷəŋən peoples on whose traditional territory the University of Victoria stands and the Songhees, Esquimalt and W̱SÁNEĆ peoples whose historical relationships with the land continue to this day. Primary financial support came from Natural Science and Engineering Research Council of Canada (NSERC) Discovery Grants to Colin Goldblatt (RGPIN-2018-05929) and Anne-Sofie Ahm (RGPIN-2022-03912). High-performance computing facilities were provided via a NSERC Research Tools and Infrastructure Grant (RTI-2020-00277).

References

Abbot, D. S., Voigt, A., Li, D., Hir, G. L., Pierrehumbert, R. T., Branson, M., et al. (2013). Robust elements of snowball Earth atmospheric circulation and oases for life. *Journal of Geophysical Research: Atmospheres*, *118*(12), 6017–6027. https://doi.org/10.1002/jgrd.50540

Abraham, C., & Goldblatt, C. (2023). Changes in relative humidity profiles over Earth's oceans in a warming climate: A satellite-data-based inference. *Journal of the Atmospheric Sciences*, *80*(7), 1847–1866. https://doi.org/10.1175/jas-d-22-0119.1

Bekker, A., & Holland, H. (2012). Oxygen overshoot and recovery during the early Paleoproterozoic. *Earth and Planetary Science Letters*, *317*, 295–304. https://doi.org/10.1016/j.epsl.2011.12.012

Bekker, A., Kaufman, A., Karhu, J., & Eriksson, K. (2005). Evidence for Paleoproterozoic cap carbonates in North America. *Precambrian Research*, *137*(3–4), 167–206. https://doi.org/10.1016/j.precamres.2005.03.009

Bekker, A., Krapež, B., & Karhu, J. A. (2020). Correlation of the stratigraphic cover of the Pilbara and Kaapvaal cratons recording the lead up to Paleoproterozoic Icehouse and the GOE. *Earth-Science Reviews*, *211*, 103389. https://doi.org/10.1016/j.earscirev.2020.103389

Catling, D., Claire, M., & Zahnle, K. (2007). Anaerobic methanotrophy and the rise of atmospheric oxygen. *Philosophical Transactions of the Royal Society A: Mathematical, Physical & Engineering Sciences*, *365*(1856), 1867–1888. https://doi.org/10.1098/rsta.2007.2047

Catling, D. C., & Zahnle, K. J. (2020). The Archean atmosphere. *Science Advances*, *6*(9), eaax1420. https://doi.org/10.1126/sciadv.aax1420

Evans, D. A., Beukes, N. J., & Kirschvink, J. L. (1997). Low-latitude glaciation in the Palaeoproterozoic era. *Nature*, *386*(6622), 262–266. https://doi.org/10.1038/386262a0

Farquhar, J., Bao, H., & Thiemens, M. (2000). Atmospheric influence of Earth's earliest sulfur cycle. *Science*, *289*(5480), 756–758. https://doi.org/10.1126/science.289.5480.756

Farquhar, J., Savarino, J., Airieau, S., & Thiemens, M. H. (2001). Observation of wavelength-sensitive mass-independent sulfur isotope effects during SO_2 photolysis: Implications for the early atmosphere. *Journal of Geophysical Research*, *106*(E12), 32829–32839. https://doi.org/10.1029/2000je001437

Garduno Ruiz, D., Goldblatt, C., & Ahm, A.-S. (2023). Climate shapes the oxygenation of Earth's atmosphere across the Great Oxidation Event. *Earth and Planetary Science Letters*, *607*, 118071. https://doi.org/10.1016/j.epsl.2023.118071

Garduno Ruiz, D., Goldblatt, C., & Ahm, A.-S. (2024a). Model output for "climate variability leads to multiple oxygenation episodes across the Great Oxidation Event". *Geophysical Research Letters [Model output]. Zenodo*. https://doi.org/10.5281/zenodo.10480761

Garduno Ruiz, D., Goldblatt, C., & Ahm, A.-S. (2024b). Software for "climate variability leads to multiple oxygenation episodes across the Great Oxidation Event" [Software]. Geophysical Research Letters. Github. Retrieved from https://github.com/DanyIvan/climate_goe_over_time

Gumsley, A. P., Chamberlain, K. R., Bleeker, W., Söderlund, U., Kock, M. O. d., Larsson, E. R., & Bekker, A. (2017). Timing and tempo of the Great Oxidation Event. *Proceedings of the National Academy of Sciences of the United States of America*, *114*(8), 1811–1816. https://doi.org/10.1073/pnas.1608824114

Guo, Q., Strauss, H., Kaufman, A. J., Schröder, S., Gutzmer, J., Wing, B., et al. (2009). Reconstructing Earth's surface oxidation across the Archean-Proterozoic transition. *Geology*, *37*(5), 399–402. https://doi.org/10.1130/g25423a.1

Hannah, J. L., Bekker, A., Stein, H. J., Markey, R. J., & Holland, H. D. (2004). Primitive Os and 2316 Ma age for marine shale: Implications for Paleoproterozoic glacial events and the rise of atmospheric oxygen. *Earth and Planetary Science Letters*, *225*(1–2), 43–52. https://doi.org/10.1016/j.epsl.2004.06.013

Harada, M., Tajika, E., & Sekine, Y. (2015). Transition to an oxygen-rich atmosphere with an extensive overshoot triggered by the Paleoproterozoic snowball Earth. *Earth and Planetary Science Letters*, *419*, 178–186. https://doi.org/10.1016/j.epsl.2015.03.005

Hir, G. L., Donnadieu, Y., Goddéris, Y., Pierrehumbert, R. T., Halverson, G. P., Macouin, M., et al. (2009). The snowball Earth aftermath: Exploring the limits of continental weathering processes. *Earth and Planetary Science Letters*, *277*(3–4), 453–463. https://doi.org/10.1016/j.epsl.2008.11.010

Izon, G., Luo, G., Uveges, B. T., Beukes, N., Kitajima, K., Ono, S., et al. (2022). Bulk and grain-scale minor sulfur isotope data reveal complexities in the dynamics of Earth's oxygenation. *Proceedings of the National Academy of Sciences of the United States of America*, *119*(13), e2025606119. https://doi.org/10.1073/pnas.2025606119

Kadoya, S., Catling, D. C., Nicklas, R. W., Puchtel, I. S., & Anbar, A. D. (2020). Mantle data imply a decline of oxidizable volcanic gases could have triggered the Great Oxidation. *Nature Communications*, *11*(1), 2774. https://doi.org/10.1038/s41467-020-16493-1

Kasting, J. F. (2013). What caused the rise of atmospheric O_2? *Chemical Geology*, *362*, 13–25. https://doi.org/10.1016/j.chemgeo.2013.05.039

Killingsworth, B. A., Sansjofre, P., Philippot, P., Cartigny, P., Thomazo, C., & Lalonde, S. V. (2019). Constraining the rise of oxygen with oxygen isotopes. *Nature Communications*, *10*(1), 4924. https://doi.org/10.1038/s41467-019-12883-2

Kirschvink, J. L. (1992). Late Proterozoic low-latitude global glaciation: The snowball Earth. In J. W. Schopf & C. Klein (Eds.), *The proterozoic biosphere: A multidisciplinary study* (pp. 51–52). Cambridge University Press. Retrieved from https://authors.library.caltech.edu/records/vaysf-cca32

Luo, G., Ono, S., Beukes, N. J., Wang, D. T., Xie, S., & Summons, R. E. (2016). Rapid oxygenation of Earth's atmosphere 2.33 billion years ago. *Science Advances*, *2*(5), e1600134. https://doi.org/10.1126/sciadv.1600134

Mills, B., Watson, A. J., Goldblatt, C., Boyle, R., & Lenton, T. M. (2011). Timing of Neoproterozoic glaciations linked to transport-limited global weathering. *Nature Geoscience*, *4*(12), 861–864. https://doi.org/10.1038/ngeo1305

Pavlov, A., & Kasting, J. (2002). Mass-independent fractionation of sulfur isotopes in Archean sediments: Strong evidence for an anoxic Archean atmosphere. *Astrobiology*, *2*(1), 27–41. https://doi.org/10.1089/153110702753621321

Philippot, P., Ávila, J. N., Killingsworth, B. A., Tessalina, S., Baton, F., Caquineau, T., et al. (2018). Globally asynchronous sulphur isotope signals require re-definition of the Great Oxidation Event. *Nature Communications*, *9*(1), 2245. https://doi.org/10.1038/s41467-018-04621-x

Popp, M., Schmidt, H., & Marotzke, J. (2016). Transition to a moist greenhouse with CO_2 and solar forcing. *Nature Communications*, *7*(1), 10627. https://doi.org/10.1038/ncomms10627

Poulton, S. W., Bekker, A., Cumming, V. M., Zerkle, A. L., Canfield, D. E., & Johnston, D. T. (2021). A 200-million-year delay in permanent atmospheric oxygenation. *Nature*, *592*(7853), 232–236. https://doi.org/10.1038/s41586-021-03393-7

Rasmussen, B., Bekker, A., & Fletcher, I. R. (2013). Correlation of Paleoproterozoic glaciations based on U–Pb zircon ages for tuff beds in the Transvaal and Huronian Supergroups. *Earth and Planetary Science Letters*, *382*, 173–180. https://doi.org/10.1016/j.epsl.2013.08.037

Reinhard, C. T., Planavsky, N. J., & Lyons, T. W. (2013). Long-term sedimentary recycling of rare sulphur isotope anomalies. *Nature*, *497*(7447), 100–103. https://doi.org/10.1038/nature12021

Schröder, S., Beukes, N. J., & Armstrong, R. A. (2016). Detrital zircon constraints on the tectonostratigraphy of the Paleoproterozoic Pretoria Group, South Africa. *Precambrian Research*, *278*, 362–393. https://doi.org/10.1016/j.precamres.2016.03.016

Senger, M., Davies, J., Ovtcharova, M., Beukes, N., Gumsley, A., Gaynor, S., et al. (2023). Improving the chronostratigraphic framework of the Transvaal Supergroup (South Africa) through in-situ and high-precision U-Pb geochronology. *Precambrian Research*, *392*, 107070. https://doi.org/10.1016/j.precamres.2023.107070

Tang, H., & Chen, Y. (2013). Global glaciations and atmospheric change at ca. 2.3 Ga. *Geoscience Frontiers*, *4*(5), 583–596. https://doi.org/10.1016/j.gsf.2013.02.003

Williams, G. E., & Schmidt, P. W. (1997). Paleomagnetism of the Paleoproterozoic Gowganda and Lorrain formations, Ontario: Low paleolatitude for Huronian glaciation. *Earth and Planetary Science Letters*, *153*(3–4), 157–169. https://doi.org/10.1016/s0012-821x(97)00181-7

Wogan, N. F., Catling, D. C., Zahnle, K. J., & Claire, M. W. (2022). Rapid timescale for an oxic transition during the Great Oxidation Event and the instability of low atmospheric O2. *Proceedings of the National Academy of Sciences of the United States of America*, *119*(37). https://doi.org/10.1073/pnas.2205618119

Zahnle, K., Claire, M., & Catling, D. (2006). The loss of mass-independent fractionation in sulfur due to a Palaeoproterozoic collapse of atmospheric methane. *Geobiology*, *4*(4), 271–283. https://doi.org/10.1111/j.1472-4669.2006.00085.x

Zeh, A., Wilson, A. H., & Gerdes, A. (2020). Zircon U-Pb-Hf isotope systematics of Transvaal Supergroup—Constraints for the geodynamic evolution of the Kaapvaal craton and its hinterland between 2.65 and 2.06 Ga. *Precambrian Research*, *345*, 105760. https://doi.org/10.1016/j.precamres.2020.105760